Journal of Neuropathology and Experimental Neurology

Vol. 60, No. 5
May, 2001
pp. 449–461

Fibroblasts Can Express Glial Fibrillary Acidic Protein (GFAP) In Vivo

JOHANNES A. HAINFELLNER, MD, TILL VOIGTLÄNDER, MD, THOMAS STRÖBEL, PHD, PETER R. MAZAL, MD, ALESSIA S. MADDALENA, MD, ADRIANO AGUZZI, MD, AND HERBERT BUDKA, MD

Abstract. Neuropathologists use anti-glial fibrillary acidic protein (GFAP) antibodies as specific markers for glial cells, and neurobiologists use GFAP for targeting transgenes to glial cells. Since GFAP has also been detected in non-glial cells, we systematically analyzed GFAP expression in human and murine non-CNS tissues using a panel of anti-GFAP antibodies. In human tissues we confirm previously observed GFAP expression in Schwann cells, myoepithelial cells, and chondrocytes, and show for the first time GFAP expression in fibroblasts of epiglottic and auricular perichondrium, ligamentum flavum, and cardiac valves. In mice we show GFAP expression in Schwann cells, bone marrow stromal cells, chondrocytes, and in fibroblasts of dura mater, skull and spinal perichondrium, and periosteum, connective stroma of oral cavity, dental pulp, and cardiac valves. Anti-GFAP immunoblotting of human non-CNS tissues reveals protein bands with a molecular mass ranging between ≈35 and ≈42 kDa. In GFAP-v-*src* transgenic mice, whose oncogenic v-*src* transgene transforms GFAP expressing cells, non-CNS tumors originate from fibroblasts. We conclude that human and murine fibroblasts can express GFAP in vivo. The somatic distribution of GFAP expressing fibroblasts indicates origin from the neural crest. Development of non-CNS tumors from fibroblasts in GFAP-v-*src* mice functionally confirms GFAP expression in these cells.

Key Words: Antibodies; Astrocytes; Fibroblasts; Glial fibrillary acidic protein analysis; Immunoblotting; Immunohistochemistry; Transgenic mice.

INTRODUCTION

Glial fibrillary acidic protein (GFAP) is a highly conserved intermediate filament protein expressed in differentiated glial cells (1). Originally thought to be expressed specifically in astrocytes, GFAP expression has also been documented in myelin marker-positive glia within the CNS (2). In clinical and experimental neuropathology, anti-GFAP antibodies are used as specific markers for glial cells and their reactive response to injury and disease, and for the discrimination of glial and non-glial cells or neoplasms (3, 4). Neurobiologists use GFAP for targeting transgenes to glial cells to create disease models (5–9). However, GFAP mRNA and protein have also been detected in non-CNS cells. These cells include enteric glia (10), satellite and Schwann cells (11, 12), chondrocytes (13, 14), myoepithelial cells of breast glands (15), human lymphocytes (16), Kupffer cells in rat liver (17), mouse bone marrow and spleen (8), rat endothelial cells (18), mouse lens epithelial cells (19), and medial layer cells of ascending aortic walls (20). GFAP expression has been shown in some non-glial neoplasms including neurofibromas (21, 22), meningiomas (13, 23, 24), pleomorphic adenomas of the salivary gland (13, 25), and a metastatic renal cell carcinoma (13).

Since GFAP is used as specific marker of glial cells or for targeting transgenes to glial cells, knowledge of GFAP expression in non-CNS tissues is of relevance to neuropathology and neurobiology. The present study is the first systematic analysis of GFAP expression in human and murine non-CNS tissues. As a novel finding we show GFAP expression in fibroblasts.

From the Institute of Neurology (JAH, TV, TS, PRM, HB), Institute of Clinical Pathology (PRM), University of Vienna, Vienna, Austria; Institute of Neuropathology (ASM, AA), University of Zurich, Zurich, Switzerland.

Correspondence to: Johannes A. Hainfellner, MD, Institute of Neurology, University of Vienna, AKH 4J, Währinger Gürtel 18-20, POB 48, A-1097 Wien, Austria.

MATERIALS AND METHODS

Human Tissues

Human tissue samples of all major body organs and systems were collected from biopsies and autopsies received for routine pathologic analysis and are listed in Table 1.

Murine Tissues

Tissues were sampled from 1) 39 C57BL/6 or sv129 wildtype mice, 2) 5 GFAP-null (GFAP^{tm1Mes}) mice (26) (The Jackson Laboratory, Bar Harbor, ME), and 3) two lines of GFAP-v-*src* transgenic mice (GFAP-v-*src*1 and GFAP-v-*src*2 lines harboring the v-*src* gene embedded within a modified full-length *GFAP* gene) (9, 27). The cohort of GFAP-v-*src* transgenic mice comprises 16 GFAP-v-*src*1 and 9 GFAP-v-*src*2 transgenic mice, and 4 TP53$^{+/-}$ GFAP-v-*src*1, 33 TP53$^{+/-}$ GFAP-v-*src*2, 17 RB-1$^{+/-}$ GFAP-v-*src*1, and 8 RB-1$^{+/-}$ GFAP-v-*src*2 transgenic mice. Details on generation and breeding of these mice have been published previously (27). The tissues include head and spine with cranial and spinal nerve roots, skeletal muscle, skin, lung, liver, pancreas, spleen, kidney, adrenal glands, ovary, testis, and gut from wildtype, GFAP-null and GFAP-v-*src* transgenic mice, respectively. In addition to non-neoplastic tissues, we analyzed GFAP-expressing non-CNS tumors in GFAP-v-*src* transgenic mice. The astrocytic tumors in these mice have been analyzed in a previous study (27). GFAP negative tumors related to TP53 or RB-1 heterozygosity (27) were excluded from the present investigation. Since neither RB-1 nor TP53 heterozygosity changes latency and frequency of GFAP expressing non-CNS tumors (27), we grouped for simplification GFAP-v-*src*, TP53$^{+/-}$ GFAP-v-*src*, and RB-1$^{+/-}$ GFAP-v-*src*

TABLE 1
Anti-GFAP Immunoreactive Cells in Human Non-CNS Tissues

Organ/tissue	Autopsy/ biopsy	No. of samples	Anti-GFAP immunoreactive cells
Integument			
Cutis	A,B	2	Myoepithelial cells of exocrine glands
Mamma	A	1	Myoepithelial cells of exocrine glands
Sole of the foot	A	1	Myoepithelial cells of exocrine glands
Face, oral cavity			
Auricular cartilage	A	1	Chondrocytes (numerous), perichondrial fibroblasts
Nose cartilage	A	1	Chondrocytes (few), myoepithelial cells, Schwann cells of nerve branches
Parotid gland	A	1	Myoepithelial cells
Submandibular gland	A	1	Myoepithelial cells, Schwann cells of nerve branches
Sublingual gland	A	1	Myoepithelial cells
Tongue	A	2	Myoepithelial cells of exocrine glands
Palate	A	1	Myoepithelial cells of exocrine glands
Neuromuscular system			
Spinal ganglion	A,B	2	Schwann cells
Nerve roots	A,B	2	Schwann cells
Sensory nerve (N. suralis)	B	3	Schwann cells
Motor nerve (N. medianus)	B	1	Schwann cells
Musculus temporalis	B	1	0
Musculus deltoideus	B	1	0
Musculus gastrocnemius	B	1	0
Musculus iliopsoas	A	1	0
Tendon of musculus iliopsoas	A	1	0
Meninges, Skeleton			
Leptomeninges	B	5	0
Dura mater (cerebral)	B	2	0
Periosteum (vertebral column)	B	1	0
Intervertebral disk	B	5	Chondrocytes (few)
Synovia (spinal joints)	B	4	0
Ligamentum flavum	B	5	Fibroblasts
Costal cartilage	A	2	Adipocytes of adherent soft tissue
Bone marrow	B	3	0
Connective tissue			
Connective membrane around bleeding	B	4	0
Cutaneous scar	B	1	0
Palmar fascia with nodular fibromatosis	B	2	0
Endocrine system			
Pituitary gland	A	1	Sustentacular cells
Thyroid gland	A	1	Schwann cells of nerve branches
Parathyroid gland	A	1	0
Adrenal gland	A	1	Schwann cells of nerve fibers
Cardiovascular system			
Cardiac muscle	A	1	0
Mitral valve	A	4	Fibroblasts, subendocardial adipocytes
Aortic valve	A	4	Fibroblasts
Tricuspid valve	A	1	Fibroblasts
Ascending aorta	A	1	Cells of medial layer
Aorta abdominalis	A	1	Schwann cells of perivasc. nerve fibers
Arteria iliaca	A	1	Schwann cells of perivasc. nerve fibers
Arteria temporalis	B	3	Schwann cells of perivasc. nerve fibers
Vena cava	A	1	Schwann cells of perivasc. nerve fibers
Leg vein	B	1	Schwann cells of perivasc. nerve fibers
Lymphatic system			
Spleen	A,B	7	Discrete dot-and threadlike immunoreacivities-Schwann cell profiles?
Lymph node	A	1	Schwann cells of perivasc. nerve fibers
Respiratory tract			
Epiglottis with mucosa	A	2	Chondrocytes, perichondrial fibroblasts, adipocytes, myoepithelial cells, Schwann cells of nerve branches

TABLE 1 (Continued)

Organ/tissue	Autopsy/ biopsy	No. of samples	Anti-GFAP immunoreactive cells
Trachea	A	1	Chondrocytes, perichondrial fibroblasts, adipocytes, myoepithelial cells, Schwann cells of nerve branches
Bronchus	A	1	Chondrocytes, perichondrial fibroblasts, adipocytes, myoepithelial cells, Schwann cells of nerve branches
Lung	A	1	Chondrocytes, perichondrial fibroblasts, Schwann cells of nerve branches
Intestines			
Esophagus	A	1	Enteric glia
Stomach	A	1	Enteric glia
Small intestine	A	1	Enteric glia
Appendix	A	1	Enteric glia
Colon	A	1	Enteric glia
Liver	A	1	Schwann cells of perivasc. nerve fibers
Pancreas	A	1	Schwann cells of nerve branches
Genitourinary tract			
Kidney	A	1	Schwann cells of nerve branches
Renal pelvis	A	1	Schwann cells of nerve branches
Ureter	A	1	Schwann cells of nerve branches
Urinary bladder	A	1	Schwann cells of nerve branches
Prostate	A	1	Schwann cells of nerve branches
Seminal vesicle	A	1	Schwann cells of nerve branches
Epididymis	A	1	Schwann cells of nerve branches
Testis	A	1	Schwann cells of nerve branches
Glans penis	A	1	Schwann cells of nerve branches
Ovary	A	1	0
Fallopian tube	A	1	Schwann cells of nerve branches
Uterus	A	1	Schwann cells of nerve branches
Vagina	A	1	Schwann cells of nerve branches

transgenic mice together and designated them in the following collectively as GFAP-v-*src*1 or GFAP-v-*src*2 transgenic mice.

Histology

Human tissues were routinely fixed in 10% formalin. Murine tissues were fixed overnight in 4% (wt/vol.) paraformaldehyde in phosphate buffered saline (PBS). Bones and spines of mice were fixed as above, then decalcified in 0.5 M EDTA, pH 8.0 for 10 days. All tissues were embedded in paraffin; 5-μm sections were cut and stained with hematoxylin and eosin.

Immunohistochemistry

A panel of monoclonal and polyclonal anti-GFAP antibodies was used. The antibodies and staining protocols are listed in Table 2. Anti-S100 protein immunostaining was performed with a polyclonal antibody (rabbit, 1:200; Dako, Glostrup, Denmark).

For immunohistochemical detection of GFAP, polyclonal antibody Z 0334 proved to be the most sensitive marker. All human and murine wildtype or transgenic tissues were first immunostained with antibody Z 0334 and meticulously screened for labeled cells. Tissue blocks that contained labeled cells were subsequently immunostained with the other anti-GFAP antibodies (Table 2). Negative controls included omission or substitution of the primary antibodies by nonspecific, isotype-matched antibodies, and immunostaining of GFAP-null tissues. To identify the cellular origin of GFAP expressing non-CNS tumors, all available tissue blocks of GFAP-v-*src* mice were screened for incipient tumors. Larger tumors in which the cellular origin was not identifiable were analyzed for involvement of surrounding non-neoplastic tissues in tumor growth.

In Situ Hybridization

The GFAP transcription vector was constructed as described previously (9). The v-*src* transcription vector was cloned by inserting the BamH I fragment from vector SR2 (28) (containing the coding sequence of the rous sarcoma virus tyrosine kinase; kind gift from Dr. E. Wagner, Institute of Molecular Pathology, Vienna, Austria) into the BamH I site of pBluescript KS II (Stratagene, La Jolla, CA) and confirming its orientation by restriction analysis.

All RNA probes were transcribed according to standard protocols, GFAP probes in antisense (T3) and sense (T7) orientation, respectively (the latter used for control staining), v-*src* probes only in antisense (T3) orientation. All probes were purified using MicroSpin-S-400 HR columns (Amersham Pharmacia Biotech, Piscataway, NJ) according to the manufacturer's protocol. In situ hybridization was performed as described previously (29) except for the following modifications: 1) proteinase K treatment was carried out prior to acetylation in 0.5% acetic anhydride; 2) hybridization temperature was generally at 65°C; and 3) hybridization time ranged between 6 and 15.5 hours (h).

TABLE 2
Anti-GFAP Antibodies and Staining Protocols for Immunohistochemistry and Immunoblotting

Clone/product no.	mc/pc	Company	Tissue pretreatment (1HC)	Antibody dilution (IHC)	Detection system (IHC)	Antibody dilution (IB)	Detection system (IB)
IHC PROTOCOLS FOR HUMAN TISSUES, IB PROTOCOLS FOR HUMAN AND MURINE TISSUES							
4A11+2E1+B4*	mc	Pharmingen (α)	citrate buffer pH 6.0, 100°C, 10 min	1:1000	ChemMate (1)	1:1000	goat anti-mouse kappa HRPO (2)
4All	mc	Pharmingen (α)	citrate buffer pH 6.0, 100°C, 10 min	1:1000	ChemMate (1)	1:1000	goat anti-mouse kappa HRPO (2)
2El	mc	Pharmingen (α)	citrate buffer pH 6.0, 100°C, 10 min	1:1000	ChemMate (1)	1:1000	goat anti-mouse kappa HRPO (2)
1B4	mc	Pharmingen (α)	citrate buffer pH 6.0, 100°C, 10 min	1:1000	ChemMate (1)	1:1000	goat anti-mouse kappa HRPO (2)
6F2+GA-5*	mc	Neomarkers (β)	citrate buffer pH 6.0, 100°C, 10 min	1:100	ChemMate (1)	1:200	goat anti-mouse kappa HRPO (2)
GA-5	mc	Neomarkers (β)	citrate buffer pH 6.0, 100°C, 10 min	1:500	ChemMate (1)	1:500	goat anti-mouse kappa HRPO (2)
6F2	mc	Dako (χ)	citrate buffer pH 6.0, 100°C, 10 min	1:100	ChemMate (1)	1:500	goat anti-mouse kappa HRPO (2)
52	mc	Transduction Lab. (Δ)	citrate buffer pH 6.0, 100°C, 10 min	1:500	ChemMate (1)	1:500	goat anti-mouse kappa HRPO (2)
GF12-24	mc	Cymbus (ϵ)	protease XXIV (1), 37°C, 5 min	1:50	ChemMate (1)	1:500	goat anti-mouse kappa HRPO (2)
Z 0334	pc (rabbit)	Dako (χ)	protease XXIV (1), 37°C, 5 min	1:4000	ChemMate (1)	1:5000	goat anti-rabbit HRPO (3)
G9269	pc (rabit)	Sigma (ϕ)	protease XXIV (1), 37°C, 5 min	1:200	PAP (1)	1:2000	goat anti-rabbit HRPO (3)
RDI-GFAPCabG	pc (goat)	RDI Incorporation (γ)	citrate buffer pH 6.0, 100°C, 10 min	1:50	ABC (1)	1:1000	donkey anti-goat HRPO (4)
sc-6170	pc (goat)	Santa Cruz (η)	citrate buffer pH 6.0, 100°C, 10 min	1:50	ABC (1)	1:1000	donkey anti-goat HRPO (4)
IHC PROTOCOLS FOR MURINE TISSUES							
Z 0334	pc (rabbit)	Dako (χ)	protease XXIV (1), 37°C, 5 min	1:400	PAP (1)		
4A11+2El+1B4*	mc	Pharmingen (α)	citrate buffer pH 6.0, 100°C, 10 min	1:100	ARK (1)		
GA-5, biotinylated	mc	Neomarkers (β)	citrate buffer pH 6.0, 100°C, 10 min	1:500	ChemMate-streptavidin (1)		

Abbreviations: mc/pc = monoclonal/polyclonal antibody; IHC = immunohistochemistry; IB = immunoblotting; HRPO = horseradish peroxidase; PAP = peroxidase-anti-peroxidase technique; ABC = avidin-biotin complex technique; ARK = animal research kit.

* Cocktail of monoclonal antibodies.

(α) San Diego, Calif., (β) Fremont, Calif., (χ) Glostrup, Denmark, (Δ) Lexington, Ky., (ϵ) Chandlersford, Hampshire, UK, (ϕ) Saint Louis, Mo., (γ) Flanders, N.J., (η) Santa Cruz, Calif.

(1) Dako, Glostrup, Denmark, (2) Harlan Sera-Lab, Indianapolis, Ind., (3) Zymed, San Francisco, Calif., (4) Santa Cruz, Santa Cruz, Calif.

Immunoblotting

For GFAP immunoblot analysis, the same antibodies were used as for immunohistochemistry (Table 2). Fresh human autopsy and biopsy tissue samples, tissue samples from wildtype and GFAP-null mice, and tumor samples from GFAP-v-*src* transgenic mice were snap-frozen in liquid nitrogen and stored at −80°C. For protein analysis, tissue was minced and lysed for 30 min at 4°C in lysis buffer (1% NP-40, 50 mM Tris, 150 mM NaCl) containing protease-inhibitors (1 mM phenylmethylsulfonylfluoride, 7.5 μg/ml aprotinin, 40 μM leupeptin, 5 μM sodium vanadate, 20 μM sodium fluoride). Lysates (50 μg per lane) were resolved by one-dimensional SDS-PAGE under reducing conditions, followed by transfer onto a 0.45-μm polyvinylidene difluoride (PVDF) membrane (Millipore, Bedford, MA) in transfer buffer at 0.2 A for 1 h (30). After transfer, residual binding sites were blocked by incubating the membrane in Tris-buffered saline (TBS) containing 5% nonfat dry milk for 1 h at room temperature. The blots were then incubated with the appropriate primary antibody in TBS with 0.05% Tween-20 (TBST) containing 5% nonfat dry milk for 16 h at 4°C. The blots were then washed 3 times for 10 min in TBST, followed by incubation with the secondary antibody conjugated to horseradish peroxidase in TBST containing 5% nonfat dry milk for 1 h at room temperature. To avoid competing signals from heavy chains of IgG and IgM in mouse tissues, we used a goat anti-mouse kappa antibody for detection of binding of the primary monoclonal antibodies (Table 2). After 3 washes for 10 min in TBST, the blots were developed using the enhanced chemiluminescence (ECL) detection system (Amersham Pharmacia Biotech) according to the manufacturer's protocol and exposed to x-ray film (Eastman Kodak, Rochester, NY).

RESULTS

Immunohistochemistry

Human Tissues: Anti-GFAP immunoreactive cells in human tissues are listed in Table 1 and are illustrated in Figure 1A–L. Cell types are determined on basis of cell morphology and distribution in tissue (31). Anti-GFAP stains Schwann cells of peripheral nerves, enteric glia, sustentacular cells of pituitary gland, myoepithelial cells of exocrine glands, chondrocytes, adipocytes, and fibroblasts of perichondrium, heart valves, and ligamentum flavum (data of ligamentum flavum not shown). None of these cells are stained in negative controls processed in parallel, after omission or substitution of the primary antibodies by nonspecific, isotype-matched antibodies (data not shown). Besides specific immunolabeling, there is non-specific binding of some of the monoclonal anti-GFAP antibodies and immunoglobulin controls to epithelial cells of exocrine glands. In peripheral nerves, anti-GFAP immunolabeling is most intense in autonomic nerves (Fig. 1H) including nerve fibers around blood vessels (Fig. 1I) and exocrine glands. GFAP-expressing myoepithelial cells are detectable in exocrine glands all over the integument. GFAP expression in chondrocytes is particularly prominent in the epiglottis (Fig. 1D) and auricular cartilage. Cartilage at other sites contains only few or no GFAP expressing chondrocytes. GFAP expression in fibroblasts is particularly prominent in cardiac valves (Fig. 1A). With different anti-GFAP antibodies, the portion of immunostained non-CNS cells is variable (Table 3). Anti-S100 protein stains Schwann cells in peripheral nerves. On serial sections of peripheral nerves, anti-S100 stained Schwann cells display same morphology and distribution in tissue as the anti-GFAP-stained cells shown in Figure 1G, H, and I, confirming the Schwann cell nature of the GFAP-stained cells (S100 data not shown). Anti-S100 also stains chondrocytes and some fibroblasts in cardiac valves and epiglottic perichondrium.

Murine Tissues: Anti-GFAP immunoreactive cells in murine tissues are listed in Table 4 and are illustrated in Figure 2A–G and K. Cell types are determined on basis of cell morphology and distribution in tissue (32). In wildtype and GFAP-v-*src* transgenic mice, GFAP expression is detectable in Schwann cells of peripheral nerves, enteric glia (data not shown), sustentacular cells of adrenal medulla (data not shown), chondrocytes, spinal bone marrow stromal cells, and in fibroblasts of dura mater, periosteum and perichondrium of skull and spinal bones, synovia of intervertebral joints (data not shown), cardiac valves, connective stroma of tongue, palate, pharynx, and dental pulp. None of these cells are stained in GFAP-null tissues or in negative controls after omission or substitution of the primary antibodies by nonspecific, isotype-matched antibodies. In the peripheral nervous system, anti-GFAP stains autonomic nerves including nerve fibers around blood vessels (Fig. 2F). In cranial and spinal nerve roots, ganglia, and peripheral nerves, only few slender cell profiles are anti-GFAP immunoreactive (data not shown). Intimate relationship of neural cell components does not allow clear-cut identification of the anti-GFAP immunolabeled profiles as Schwann cells or fibroblasts. Anti-S100 protein stains Schwann cells in peripheral nerves, chondrocytes, and a few fibroblasts in periosteum and perichondrium of skull and spinal bones, and connective stroma of the oral cavity (data not shown).

In GFAP-v-*src* mice, early tumors originating from fibroblasts are detectable in leptomeninges, dura mater (Fig. 2I), periosteum and perichondrium of skull and spinal bones and cartilage (Fig. 2L), peri- and endoneurium of cranial and spinal nerve roots/ganglia/nerves and sympathetic trunk, endomysium of skeletal muscle, fibrous septae of adipose tissue, connective stroma of internal organs (thymus, spleen, pancreas), perivascular connective tissue, and (sub-)cutis (Tables 4, 5).

Furthermore, we observed early tumors arising from enteric glia and spinal bone marrow stromal cells (data not shown). Advanced tumor growth occurs mainly in

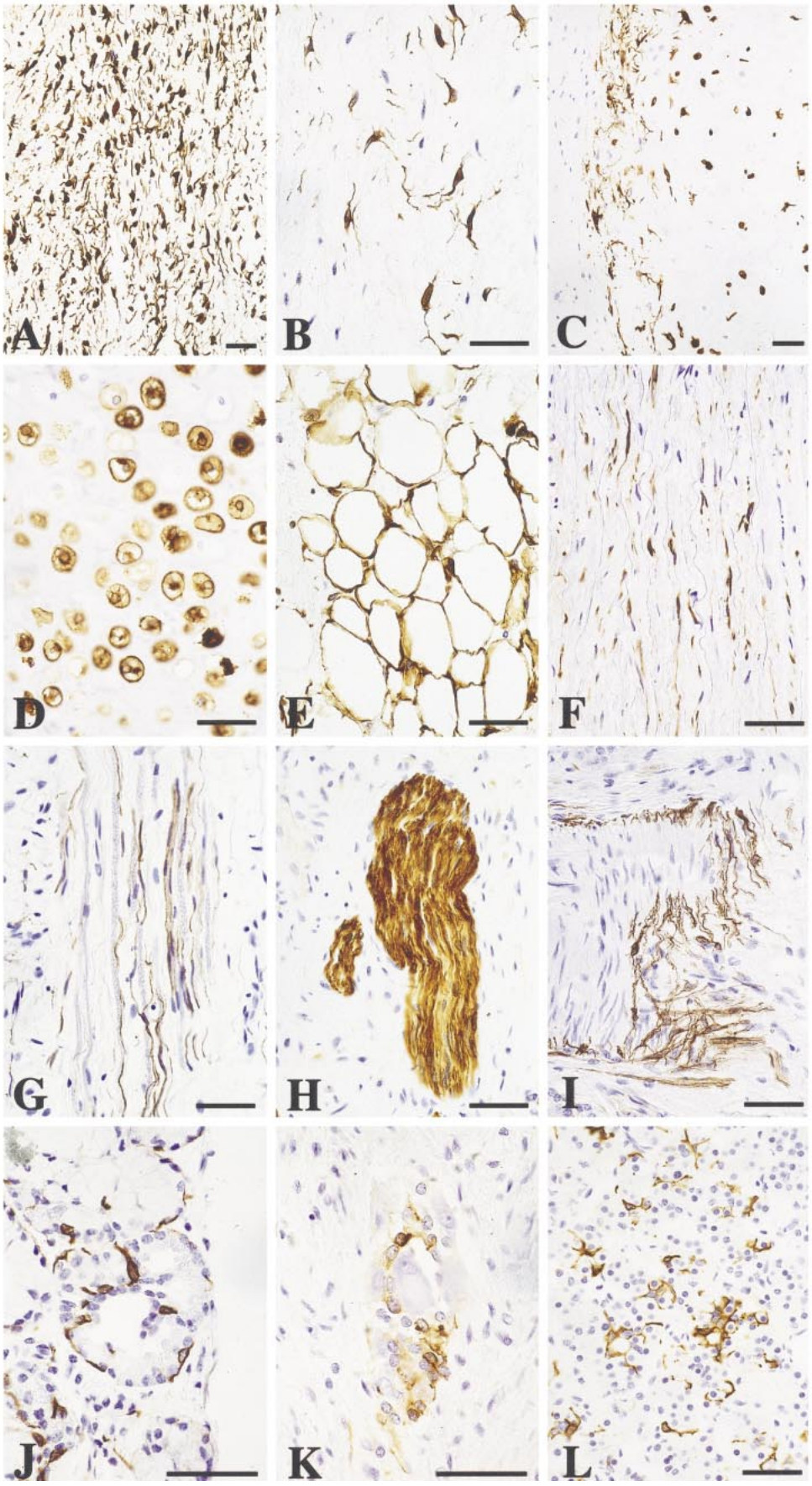

the head and truncal regions and involves the leptomeninges, dura mater (Fig. 2J), periosteum (Fig. 2M), perichondrium, endo- and perineurium of nerve roots and ganglia, and bone marrow. Other tumors involve paraspinal soft tissue and the retroperitoneum (endomysium of skeletal muscles, perivascular connective tissue, adipose tissue, and sympathetic trunk), retrobulbar space (endomysium of ocular muscles, adipose tissue, and ciliary ganglion), oral cavity (tongue, palate, and lip), stomach and gut, connective stroma of internal organs (lung, pancreas, liver, and spleen), and connective/adipose tissue of (sub-)cutis (data not shown). The non-CNS tumors show a similar somatic distribution in GFAP-v-*src*1 and GFAP-v-*src*2 mice, but are more widespread in GFAP-v-*src*2 mice (Table 5). The cytological spectrum of tumor cells comprises spindle-shaped forms, large-bodied cells with eccentric nuclei, and pleomorphic cells. In most tumors, anti-GFAP antibodies bind to the majority of tumor cells. Some tumors contain areas devoid of anti-GFAP binding, or only a minority of tumor cells shows GFAP staining (data not shown). In the total cohort of 87 tumor-bearing mice, prominent S100 protein expression as indicator of Schwann cell origin is restricted to a small portion of the tumors. These tumors comprise 3 neoplasms originating from plexus myentericus of gut and stomach, 1 skin tumor, 1 tumor of spinal nerve root, and 1 tumor in the retrobulbar space. The other tumors show only faint anti-S100 immunoreactivity in a few tumor cells or no immunostaining at all (data not shown).

In Situ Hybridization

In situ hybridization studies of GFAP were performed on murine tissues. In preliminary experiments the specificity of in situ hybridization for GFAP was controlled with sense and antisense probes on a brain of a wildtype mouse and a brain of a GFAP-v-*src* transgenic mouse containing an astrocytic tumor with immunohistochemically confirmed GFAP expression. The sense probe did not yield positive hybridization signals, whereas the antisense probe hybridized to a portion of astrocytes in the wildtype brain and showed prominent signals in the astrocytic tumor. The specificity of the GFAP antisense probe was also controlled on a block of a GFAP expressing skin tumor. The skin tumor contained focal areas devoid of immunohistochemical GFAP expression. Hybridization of the GFAP antisense probe was restricted to areas with immunohistochemically detectable GFAP. We also analyzed the expression of v-*src* mRNA. The specificity of v-*src* in situ hybridization was controlled with v-*src* antisense probes on tissues from v-*src* transgenic animals (astrocytic brain tumor and fibroblastic skin tumor) and from wildtype mice (brain). The antisense probe hybridized selectively to tumor cells in transgenic mice.

We then performed in situ hybridization on selected tissue specimens of GFAP-v-*src* and wildtype mice. Specimens of transgenic mice contained early and advanced anti-GFAP immunoreactive non-CNS tumors originating from fibroblasts of the meninges, endo- and perineurium of nerve roots and peripheral nerves, and skull- and spinal periosteum and perichondrium. The specimens of wildtype mice contained GFAP expressing fibroblasts of cardiac valves, spinal synovia and periosteum, and connective stroma of the oral cavity. In GFAP-v-*src* mice, the non-CNS tumors show expression of GFAP mRNA (Fig. 2H) and v-*src* mRNA. In tissues of wildtype mice, GFAP transcripts are detectable in Müller's cells of retina and astrocytes of optic nerves, but not in fibroblasts that show immunohistochemically detectable GFAP expression on adjacent sections (data not shown). We consider a low rate of GFAP synthesis in non-neoplastic fibroblasts as cause for the absence of GFAP transcripts.

Immunoblotting

Immunoblotting was performed to determine the molecular mass of GFAP expressed in human and murine brains and non-CNS tissues, and in tumors of GFAP-v-*src* mice. In preliminary immunoblot experiments using human or murine brain, or non-CNS tissues, the polyclonal anti-GFAP antibodies (Table 2) detected bands that were not interpretable, in addition to bands consistent with GFAP. Antibody Z 0334 stained numerous bands all over the lanes even in GFAP-null brains (data not

←

Fig. 1. Anti-GFAP immunoreactive cells in human non-CNS tissues. Fibroblasts in cardiac valves (A, B). Low magnification (A) illustrates the focally high cellular density and scattered distribution of labeled cells. Higher magnification (B) shows cytological details of labeled cells with slender processes embedded in connective stroma. Distribution in tissue in conjunction with cell morphology define these cells as fibroblasts. Perichondrial fibroblasts (C) and chondrocytes (C and D) of epiglottis. Low magnification (C) shows perichondrium (left-hand part of the figure) abutting on cartilage (right-hand part of the figure). The perichondrium contains scattered immunolabeled cells with slender processes embedded in connective stroma. Distribution in tissue in conjunction with cell morphology define these cells as fibroblasts. Subendocardial adipocytes (E). Medial layer cells of ascending aorta (F). Schwann cells, low density of immunolabeled cells in nervus medianus (G), high density of labeled cells in autonomic nerves of glandula seminalis (H). Schwann cells of perivascular nerve fibers (I). Myoepithelial cells of exocrine glands (J). Enteric glia of gut (K). Sustentacular cells of pituitary gland (L). Anti-GFAP antibody used in Figure 1: Z 0334. Scale bars: 50 μm.

TABLE 3
Anti-GFAP Immunostaining of Human Non-CNS Cells

	Anti-GFAP antibodies												
	4All	2El	1B4	4A11, 2E1, 1B4*	GA-5	6F2	6F2, GA-5*	52	GF12-24	Z0334	G9269	RDI-GFAP-CabG	sc-6170
Epiglottis:													
Chondrocytes	3	3	3	3	2	3	3	2	2	3	3	2	2
Perichondrial fibroblasts	2	2	2	2	2	2	2	2	1	3	3	1	1
Adipocytes	1	1	1	1	1	1	1	1	0	2	2	0	0
Myoepithelial cells	1	1	1	1	1	2	2	2	0	2	2	0	0
Mitral valve:													
Fibroblasts	3	3	3	3	2	3	3	1	1	3	3	1	2
Subendocardial adipocytes	1	1	1	1	1	3	3	0	0	3	2	1	1
Ligamentum flavum:													
Fibroblasts	2	2	2	2	2	2	2	2	0	2	2	0	1
Seminal vesicle:													
Schwann cells of autonomic nerves	2	2	2	2	2	3	3	nd	0	3	3	0	0
Nervus medianus:													
Schwann cells of motor/sensory nerve	0	0	0	0	0	2	2	nd	0	3	1	0	0

* Cocktail of monoclonal antibodies.
0 = no cells; 1 = few cells; 2 = some cells; 3 = numerous cells immunolabeled; nd = not done.

shown). The monoclonal antibodies, however, showed no unclear additional bands. Immunoblotting was thus performed with monoclonal anti-GFAP antibodies. Results of GFAP immunoblotting of human tissues are summarized in Table 6 and representative immunoblots of human and murine tissues are shown in Figure 3. The antibodies 4A11, 2E1, and 1B4, or a cocktail of these monoclonal antibodies, detect distinct bands consistent with the size of GFAP both in brain and non-CNS tissues. The other monoclonal antibodies detect GFAP bands only in the brain. In brain, the bands range between ≈35 and ≈48 kDa, whereas the bands in non-CNS tissues range between ≈35 and ≈42 kDa. All human non-CNS tissue samples analyzed show GFAP bands except for cardiac muscle (Table 6; Fig. 3B, C). The bands are variably intense in different tissue samples (Fig. 3B). The bands of brain tissue are more numerous and show a wider range of the molecular mass than the bands of non-CNS tissues (Fig. 3B, C).

In murine brains, cocktails of monoclonal antibodies 4A11+2E1+1B4 or 6F2+GA-5 detect immunoreactive bands ranging between ≈37 and ≈48 kDa, whereas no bands are detectable in wildtype gut and spleen or GFAP-null brains (Fig. 3A). In non-CNS tumors of GFAP-v-*src* transgenic mice, the anti-GFAP antibodies reveal immunoreactive bands showing the same range of the molecular mass as observed in brain (≈37 to ≈48 kDa; Fig. 3A). Even after long exposure, no bands with a higher molecular mass consistent with the size of a GFAP-v-*src* fusion protein were detectable. Since the v-*src* gene is embedded within a full-length *GFAP* gene, the expected molecular mass of a GFAP-v-*src* fusion protein would represent ≈110 kDa (sum of molecular masses of GFAP and v-*src* protein).

DISCUSSION

Although GFAP expression has been described in various non-CNS cells (10, 12–15), we present here the first systematic study of GFAP expression in non-CNS tissues. Using a panel of poly- and monoclonal anti-GFAP antibodies, we confirm previously observed GFAP expression in Schwann cells, myoepithelial cells of exocrine glands, and chondrocytes. As a novel finding, we show GFAP expression in fibroblasts of epiglottic and auricular perichondrium, ligamentum flavum, and cardiac valves. In mice, GFAP expressing fibroblasts are detectable in dura mater, skull and spinal perichondrium and periosteum, connective stroma of palate, pharynx and tongue, dental pulp, and cardiac valves. This somatic distribution and S100 protein expression in some of the fibroblasts indicates an origin from the neural crest. The neural crest gives rise to the connective stroma of the oral cavity, dental pulp, cardiac valves, and contributes mesenchymal cells to the meninges, skeleton, loose connective tissue, and dermis, particularly in the head, neck, and truncal regions (33–35).

In clinical and experimental neuropathology, anti-GFAP immunohistochemistry is an important tool for the discrimination of glial and non-glial cells or neoplasms (3, 4). However, we show here that human and murine fibroblasts can express immunohistochemically detectable GFAP. We controlled the specificity of this staining

TABLE 4
Anti-GFAP Immunoreactive Non-CNS Cells in Wildtype and GFAP-v-*src* Transgenic Mice

Organ/tissue	Anti-GFAP immunoreactive cell	Anti-GFAP antibody		
		Z 0334	GA5	4All+2El+1B4°
Head				
Pituitary gland	0	0	0	0
Dura mater*	Fibroblasts**	1	0	0
Periosteum*	Fibroblasts**	2	1	0
Cartilage	Chondrocytes, perichondrial fibroblasts**	2	1	0
Cranial ganglia*	Endoneurial cells#,**	1	1	0
Cranial nerve roots*	Endoneurial cells#,**	2	1	0
Nerves*	Endoneurial cells#,**	2	1	0
Palate*	Fibroblasts of connective stroma**	3	2	2
Tongue*	Fibroblasts of connective stroma**	2	1	1
Dental pulp	Fibroblasts	1	0	0
Pharynx	Fibroblasts of connective stroma	2	nd	nd
Skin*	0	0	0	0
Spine				
Meninges*	Fibroblasts of dura mater**	0	0	0
Periosteum*	Fibroblasts**	2	1	1
Cartilage	Chondrocytes	1	1	1
Perichondrium*	Fibroblasts**	2	1	1
Spinal ganglia*	Endoneurial cells#,**	1	1	0
Spinal nerve roots*	Endoneurial cells#,**	1	1	0
Nerves*	Endoneurial cells#,**	2	1	0
Bone marrow*	Bone marrow stromal cells**	2	2	1
Internal organs				
Cardiac muscle	0	0	0	0
Cardiac valves	Fibroblasts	2	1	1
Lung*	Schwann cells of perivascular nerve fibers	1	0	0
Liver	Schwann cells of perivascular nerve fibers	1	0	0
Spleen*	Schwann cells of nerve fibers	2	0	0
Kidney	Schwann cells of perivascular nerve fibers	1	0	0
Adrenal gland	Sustentacular cells	3	2	0
Gut*	Enteric glia**	3	2	1
Ovary	0	0	0	0
Testis	0	0	0	0

Cellular origin of non-CNS tumors in GFAP-v-*src* transgenic mice and tissues involved in tumor growth are indicated.
* Tissues that contain GFAP expressing non-CNS tumors in GFAP-v-*src* transgenic mice.
** Cellular source of GFAP expressing non-CNS tumors in GFAP-v*src* transgenic mice.
° Cocktail of monoclonal antibodies.
# Slender anti-GFAP immunoreactive cell profiles; intimate relationship of cellular components does not allow clear-cut identification as Schwann cells or endoneurial fibroblasts.
0 = no; 1 = few, 2 = some; 3 = numerous anti-GFAP immunoreactive cells; nd = not done.

result carefully by omission or substitution of the primary antibodies by nonspecific, isotype-matched antibodies, and immunostaining of GFAP-null tissues. In GFAP-v-*src* transgenic mice, fibroblasts of skull and spinal periosteum, the meninges and nerve roots give rise to GFAP expressing non-CNS tumors. The cellular origin of non-CNS tumors from fibroblasts in GFAP-v-*src* mice functionally confirms GFAP expression in these cells. In man, GFAP expression has been shown in single meningiomas and some neurofibromas (13, 21–24). Thus, GFAP detection in tumor biopsy samples may not be the absolute proof of a glial origin. This is relevant to the typing of histogenetically unclear tumors associated with meninges, nerve roots, or (para-)spinal soft tissues.

In addition to anti-GFAP immunohistochemistry, we performed immunoblotting to determine the molecular mass of GFAP expressed in brain and non-CNS tissues, and in tumors of GFAP-v-*src* mice. We used monoclonal anti-GFAP antibodies for immunoblotting, because the polyclonal anti-GFAP antibodies detected bands that were not interpretable, in addition to bands consistent with GFAP. In our study, anti-GFAP immunoblotting of human brain or various non-CNS tissues reveals protein bands of 35≈ to ≈48 kDa or 35≈ to ≈42 kDa, respectively. The molecular mass is consistent with GFAP (16). In human brain, 7/7 monoclonal antibodies detect GFAP bands, whereas only 3/7 antibodies reveal GFAP in human non-CNS tissues. Bands compatible with GFAP are

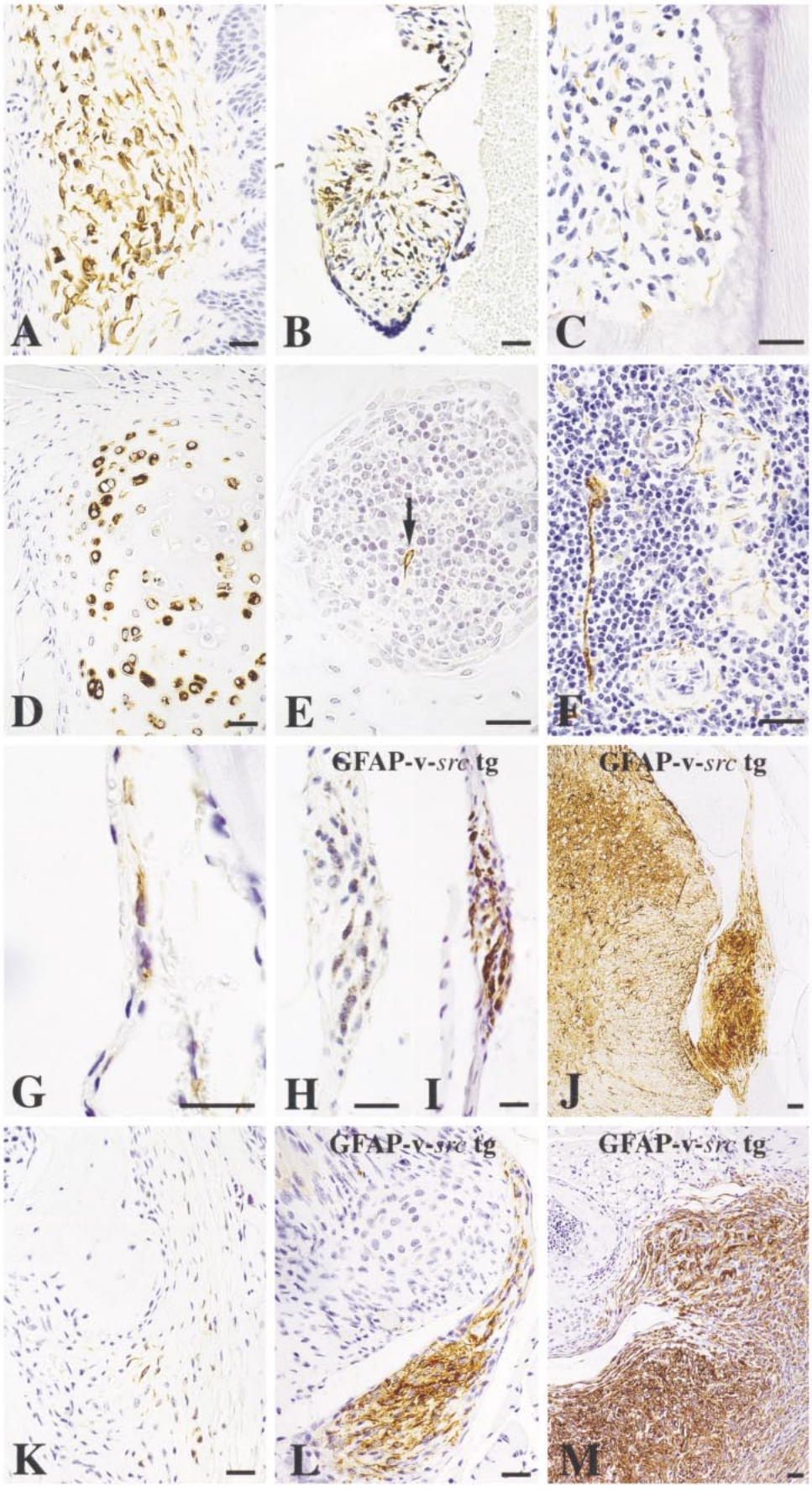

more numerous in brain showing a wider range of the molecular mass than in non-CNS tissues. Using the same anti-GFAP antibodies for immunohistochemistry, all antibodies show prominent staining of brain tissue, whereas labeling of non-CNS cells is variable. Discrepant immunoreactivity of anti-GFAP antibodies in brain and non-CNS tissues has also been reported by others (11, 16, 36). Among non-CNS cells, Schwann cells and lymphocytes have been shown to express a ß-type GFAP mRNA that is longer than the brain α-type but gives rise to a shorter protein of ≈41 kDa (8, 16, 37). Collectively, these observations indicate antigenic differences of GFAP expressed in brain and non-CNS tissues.

In our study, anti-GFAP antibodies suitable for immunohistochemistry were not necessarily as suitable for immunoblotting. For instance, the polyclonal antibody Z 0334 proved to be a very sensitive immunohistochemical marker, distinctly labeling GFAP expressing cells. On immunoblots, however, antibody Z 0334 stains even in GFAP-null brains numerous bands all over the lanes, thus not allowing proper interpretation of the blots. Furthermore, although all anti-GFAP antibodies immunostain specifically at least a few non-CNS cells, only 3/7 monoclonal antibodies detect GFAP bands on immunoblots of non-CNS tissues. One explanation for this discrepancy may be a lower sensitivity of GFAP detection on immunoblots as compared to immunohistochemistry; immunohistochemistry allows GFAP detection at the single-cell level, whereas in homogenates of non-CNS tissues used for immunoblot analysis, the relative amount of GFAP seems to be very low as compared to other proteins, such as collagen.

In GFAP-v-*src* mice, the v-*src* gene is embedded within a modified full-length *GFAP* gene. A polyadenylation signal and a translational stop codon at the 3′ end of the v-*src* sequence prevent GFAP expression from the transgene (6, 9). Expression of a GFAP-v-*src* fusion protein would yield a protein band of approximately 110 kDa (sum of the molecular masses of GFAP and v-*src* protein). Immunoblots of GFAP-v-*src* transgenic non-CNS tumors show bands of ≈37 to ≈48 kDa consistent with endogenous GFAP but not a heavier band indicative of a fusion protein from the construct.

TABLE 5
Distribution of GFAP-positive Non-CNS Tumors in GFAP-v-*src* Transgenic Mice

	GFAP-v-*src* 1 mice* (n = 37)	GFAP-v-*src* 2 mice* (n = 50)
Leptomeninges	32 (86.5%)	13 (26%)
Dura mater	2 (5.4%)	6 (12%)
Skull/spinal periosteum	2 (5.4%)	14 (28%)
Skull/spinal perichondrium	1 (2.7%)	4 (8%)
Spinal bone marrow	1 (2.7%)	6 (12%)
Cranial/spinal nerve roots	14 (37.8%)	27 (54%)
Sympathetic trunk	0	1 (2%)
Oral cavity	0	1 (2%)
Stomach/gut	3 (8.1%)	1 (2%)
Internal organs**	0	3 (6%)
Skeletal muscle	1 (2.7%)	21 (42%)
Cutis/subcutis	0	11 (22%)

* A portion of mice had more than 1 tumor, or tumors involved several tissues/organs.

** Spleen, liver, pancreas.

The GFAP-v-*src* mouse and other mouse models containing transgenes with GFAP regulatory elements have been established with the aim of targeting transgene expression specifically to glial cells (5–7, 9). In these models, RT-PCR detected transgene and GFAP transcripts in various non-CNS tissues (7, 9). Schwann cells of peripheral nerve branches that are known to express GFAP (38, 39) have been considered as the source of transgene and GFAP transcripts (9). We show here GFAP expression in murine wildtype fibroblasts, in addition to immunolabeling of enteric glia and Schwann cells. In GFAP-v-*src* transgenic mice, fibroblasts give rise to non-CNS tumors expressing GFAP-mRNA and -protein. Thus transgene expression under the control of GFAP regulatory elements targets not only glial but also mesenchymal cells.

ACKNOWLEDGMENTS

We thank Drs. Susanna Lang, Reinhard Horvat and Andreas Chott for providing some of the human tissue samples, and Helga Flicker, Christine Karner, Michaela Strohschneider, and Birgit Schmid for excellent technical assistance.

Dedication: This study is dedicated to the memory of the first author's father, Johann Gottfried Hainfellner, who succumbed to severe illness on August 4, 2000.

←

Fig. 2. A–G, K: Anti-GFAP immunoreactive cells in murine wildtype non-CNS tissues. Fibroblasts in connective stroma of hard palate (A), aortic valve (B), dental pulp (C), dura mater (G), and spinal periosteum (K). The tissues contain scattered immunolabeled cells with slender processes embedded in connective stroma. Distribution in tissue in conjunction with cell morphology define these cells as fibroblasts. Chondrocytes in cartilage of processus spinosus (D). Stromal cell of spinal bone marrow (E, arrow). Schwann cells in autonomic nerves and perivascular nerve fibers of spleen (F). H–J, L, M: Fibroblast-derived tumors showing GFAP expression in GFAP-v-*src* transgenic mice. An early dura mater tumor shows cytoplasmic hybridization signals for GFAP mRNA (H, dark dots) and GFAP protein immunostaining (I). An advanced dura mater tumor compressing the spinal cord (J). Early tumor in spinal perichondrium (L). Advanced tumor of spinal periosteum (M). Anti-GFAP immunostaining (I, J, L, M) and in-situ hybridization for GFAP mRNA (H). Anti-GFAP antibody used in Figure 2: Z 0334. Scale bars: 25 μm.

TABLE 6
Results of GFAP Immunoblotting of Human Tissues Using Monoclonal Anti-GFAP Antibodies

	Anti-GFAP antibodies								
	4A11	2E1	1B4	4A11 + 2E1 + 1B4*	6F2	GA-5	6F2 + GA-5*	GF12-24	52
Brain	+	+	+	+	+	+	+	+	+
Cardiac valves	+	+	+	+	−	−	−	−	−
Epiglottis	+	+	+	+	−	−	−	−	−
Gut	+	+	+	+	−	−	−	−	−
Seminal vesicle	+	+	+	+	−	−	−	−	−
Spleen	+	+	+	+	−	−	−	−	−
Cardiac muscle	−	−	−	−	−	−	−	−	−

* Cocktail of monoclonal antibodies.
+ = detection of protein bands consistent with GFAP.
− = lack of protein bands consistent with GFAP.

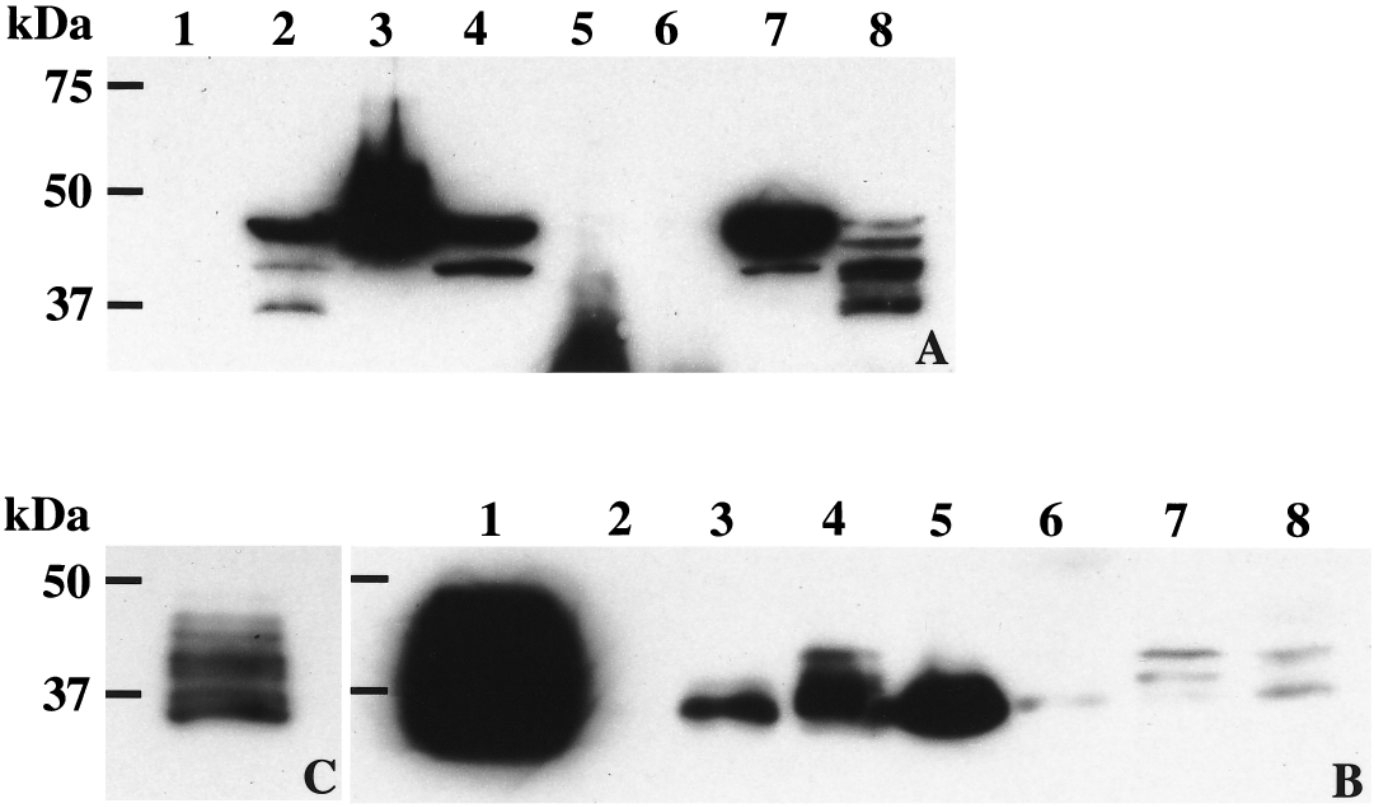

Fig. 3. A–C: Anti-GFAP immunoblot analysis of murine (A) and human (B, C) brain and non-CNS tissues. A cocktail of monoclonal antibodies 4A11, 1B4, and 2E1 was used for GFAP immunodetection both in murine and human tissues. A: Lanes 1–8 show immunoblots of GFAP-null brain (1), wildtype brains (2, 3), GFAP-v-*src* transgenic brain (4), wildtype gut (5), wildtype spleen (6), non-CNS tumors of thoracic region (7), and stomach (8) in GFAP-v-*src* transgenic mice. In wildtype (2, 3) and GFAP-v-*src* transgenic brains (4), the molecular mass of the bands ranges between ≈37 and ≈48 kDa, whereas no bands are detectable in wildtype gut (5) or spleen (6), or in the GFAP-null brain (1). In non-CNS tumors of GFAP-v-*src* transgenic mice, GFAP shows a mass of ≈37 to ≈48 kDa. Even after long exposure, no bands with a higher molecular mass were detectable. The immunoblot of the gut (5) shows a smear of immunoglobulin light-chains (but no heavy chains) because of the use of a goat anti-mouse kappa as secondary antibody. B: Lanes 1–8 show immunoblots of human brain (1), cardiac muscle (2), gut (3), seminal vesicle (4), spleen (5), submandibular gland (6), epiglottic cartilage (7), and mitral valve (8). In brain the molecular mass of the bands ranges between ≈35 and ≈48 kDa (1), whereas the bands range between ≈35 and ≈42 kDa in non-CNS tissues (2–8). GFAP bands of variable intensity are detectable in all non-CNS tissue samples analyzed except for cardiac muscle (2). C: Shows the brain immunoblot of lane 1 in (B) after short exposure. The bands are more numerous and show a wider range of the molecular mass than in non-CNS tissues.

REFERENCES

1. Brenner M, Kisseberth WC, Su Y, Besnard F, Messing A. GFAP promoter directs astrocyte-specific expression in transgenic mice. J Neurosci 1994;14:1030–37
2. Dyer CA, Kendler A, Jean Guillaume D, et al. GFAP-positive and myelin marker-positive glia in normal and pathologic environments. J Neurosci Res 2000;60:412–26
3. Sampson JH, Bigner DD. Experimental tumors and the evaluation of neurocarcinogens. In: Bigner DD, McLendon JM, eds. Russell & Rubinstein's pathology of tumors of the nervous system. 6th ed. London: Arnold, 1998:141–66, Vol 1.
4. McLendon RE, Bigner DD. Immunohistochemistry of the glial fibrillary acidic protein: Basic and applied considerations. Brain Pathol 1994;4:221–28
5. Campbell IL, Abraham CR, Masliah E, et al. Neurologic disease induced in transgenic mice by cerebral overexpression of interleukin 6. Proc Natl Acad Sci USA 1993;90:10061–65
6. Toggas SM, Masliah E, Rockenstein EM, Rall GF, Abraham CR, Mucke L. Central nervous system damage produced by expression of the HIV-1 coat protein gp120 in transgenic mice. Nature 1994; 367:188–93
7. Bush TG, Savidge TC, Freeman TC, et al. Fulminant jejuno-ileitis following ablation of enteric glia in adult transgenic mice. Cell 1998;93:189–201
8. Brenner M. Structure and transcriptional regulation of the GFAP gene. Brain Pathol 1994;4:245–57
9. Weissenberger J, Steinbach JP, Malin G, Spada S, Rulicke T, Aguzzi A. Development and malignant progression of astrocytomas in GFAP-v-src transgenic mice. Oncogene 1997;14:2005–13
10. Jessen KR, Mirsky R. Glial cells in the enteric nervous system contain glial fibrillary acidic protein. Nature 1980;286:736–37
11. Jessen KR, Thorpe R, Mirsky R. Molecular identity, distribution and heterogeneity of glial fibrillary acidic protein: An immunoblotting and immunohistochemical study of Schwann cells, satellite cells, enteric glia and astrocytes. J Neurocytol 1984;13:187–200
12. Fields KL, Yen SH. A subset of Schwann cells in peripheral nerves contain a 50-kDa protein antigenically related to astrocyte intermediate filaments. J Neuroimmunol 1985;8:311–30
13. Budka H. Non-glial specificities of immunocytochemistry for the glial fibrillary acidic protein (GFAP). Triple expression of GFAP, vimentin and cytokeratins in papillary meningioma and metastasizing renal carcinoma. Acta Neuropathol 1986;72:43–54
14. Kepes JJ, Rubinstein LJ, Chiang H. The role of astrocytes in the formation of cartilage in gliomas. An immunohistochemical study of four cases. Am J Pathol 1984;117:471–83
15. Viale G, Gambacorta M, Coggi G, Dell'Orto P, Milani M, Doglioni C. Glial fibrillary acidic protein immunoreactivity in normal and diseased human breast. Virchows Arch A Pathol Anat Histopathol 1991;418:339–48
16. Riol H, Tardy M, Rolland B, Levesque G, Murthy MR. Detection of the peripheral nervous system (PNS)-type glial fibrillary acidic protein (GFAP) and its mRNA in human lymphocytes. J Neurosci Res 1997;48:53–62
17. Gard AL, White FP, Dutton GR. Extra-neural glial fibrillary acidic protein (GFAP) immunoreactivity in perisinusoidal stellate cells of rat liver. J Neuroimmunol 1985;8:359–75
18. Schinke M, Baltatu O, Bohm M, et al. Blood pressure reduction and diabetes insipidus in transgenic rats deficient in brain angiotensinogen. Proc Natl Acad Sci USA 1999;96:3975–80
19. Boyer S, Montagutelli X, Gomes D, Simon Chazottes D, Guenet JL, Dupouey P. Recent evolutionary origin of the expression of the glial fibrillary acidic protein (GFAP) in lens epithelial cells. A molecular and genetic analysis of various mouse species. Brain Res Mol Brain Res 1991;10:159–66
20. Bonderman D, Gharehbaghi Schnell E, et al. Mechanisms underlying aortic dilatation in congenital aortic valve malformation. Circulation 1999;99:2138–43
21. Kawahara E, Oda Y, Ooi A, Katsuda S, Nakanishi I, Umeda S. Expression of glial fibrillary acidic protein (GFAP) in peripheral nerve sheath tumors. A comparative study of immunoreactivity of GFAP, vimentin, S-100 protein, and neurofilament in 38 schwannomas and 18 neurofibromas. Am J Surg Pathol 1988;12:115–20
22. Gray MH, Rosenberg AE, Dickersin GR, Bhan AK. Glial fibrillary acidic protein and keratin expression by benign and malignant nerve sheath tumors. Hum Pathol 1989;20:1089–96
23. Su M, Ono K, Tanaka R, Takahashi H. An unusual meningioma variant with glial fibrillary acidic protein expression. Acta Neuropathol Berl 1997;94:499–503
24. Wanschitz J, Schmidbauer M, Maier H, Rossler K, Vorkapic P, Budka H. Suprasellar meningioma with expression of glial fibrillary acidic protein: A peculiar variant. Acta Neuropathol 1995;90:539–44
25. Nakazato Y, Ishizeki J, Takahashi K, Yamaguchi H, Kamei T, Mori T. Localization of S-100 protein and glial fibrillary acidic protein-related antigen in pleomorphic adenoma of the salivary glands. Lab Invest 1982;46:621–26
26. McCall MA, Gregg RG, Behringer RR, et al. Targeted deletion in astrocyte intermediate filament (Gfap) alters neuronal physiology. Proc Natl Acad Sci USA 1996;93:6361–66
27. Maddalena AS, Hainfellner JA, Hegi ME, Glatzel M, Aguzzi A. No complementation between TP53 or RB-1 and v-src in astrocytomas of GFAP-v-src transgenic mice. Brain Pathol 1999;9:627–37
28. Boulter CA, Wagner EF. The effects of v-src expression on the differentiation of embryonal carcinoma cells. Oncogene 1988;2: 207–14
29. Breitschopf H, Suchanek G, Gould RM, Colman DR, Lassmann H. In situ hybridization with digoxigenin-labeled probes: Sensitive and reliable detection method applied to myelinating rat brain. Acta Neuropathol 1992;84:581–87
30. Strobel T, Swanson L, Korsmeyer S, Cannistra SA. BAX enhances paclitaxel-induced apoptosis through a p53-independent pathway. Proc Natl Acad Sci USA 1996;93:14094–99
31. Williams PL, ed. Gray's anatomy. The anatomical basis of medicine and surgery. 38th ed. Edinburgh: Churchill Livingstone, 1995
32. Welsch U, Storch V. Comparative animal cytology and histology. London: Sidgwick & Jackson, 1976
33. Le Douarin N. The neural crest.Cambridge: Cambridge University Press, 1982
34. Le Douarin NM, Dupin E. Cell lineage analysis in neural crest ontogeny. J Neurobiol 1993;24:146–61
35. O'Rahilly R, Muller F. The meninges in human development. J Neuropathol Exp Neurol 1986;45:588–608
36. Mokuno K, Kamholz J, Behrman T, et al. Neuronal modulation of Schwann cell glial fibrillary acidic protein (GFAP). J Neurosci Res 1989;23:396–405
37. Feinstein DL, Weinmaster GA, Milner RJ. Isolation of cDNA clones encoding rat glial fibrillary acidic protein: Expression in astrocytes and in Schwann cells. J Neurosci Res 1992;32:1–14
38. Jessen KR, Mirsky R. Glial fibrillary acidic polypeptides in peripheral glia. Molecular weight, heterogeneity and distribution. J Neuroimmunol 1985;8:377–93
39. Mancardi GL, Cadoni A, Tabaton M, et al. Schwann cell GFAP expression increases in axonal neuropathies. J Neurol Sci 1991;102: 177–83

Received October 11, 2000
Revision received January 8, 2001
Accepted February 6, 2001